SEMARAK ILMU PUBLISHING

CFD Letters

Journal homepage:
https://semarakilmu.com.my/journals/index.php/CFD_Letters/index
ISSN: 2180-1363

A Study of Geometrical Effects on Permeability Estimation in Three-Dimensional Fractures using the Lattice Boltzmann Method

Fatimah Az-Zahra[1,2], Irwan Ary Dharmawan[1,*]

[1] Department of Geophysics, Universitas Padjadjaran, Sumedang, Indonesia
[2] Postgraduate Physics Study Program, Universitas Padjadjaran, Sumedang, Indonesia

ARTICLE INFO

Article history:
Received 11 April 2023
Received in revised form 9 May 2023
Accepted 12 June 2023
Available online 1 December 2023

Keywords:
Fractures; Lattice Boltzmann Method; Mean aperture; Permeability; Surface roughness

ABSTRACT

This study investigates the effect of geometry on permeability estimation in three-dimensional fractures using the Lattice Boltzmann Method. Fractures have irregular and complex shapes, which can significantly impact their permeability. Anisotropy of permeability is important as it indicates the influence of changes in fracture orientation on the flow and transport properties of fluids. To examine the relationship between permeability and fracture geometry, we generated three-dimensional fracture geometries using fractal Brownian motion with a Hurst exponent to describe the roughness on the fracture surface. The fractures in this study have varying mean aperture, ranging from narrow to wide, with surface roughness that can be either uniform or non-uniform. The Lattice Boltzmann Method was performed to calculate permeability and investigate the relationship between permeability and geometric parameters of fractures, such as mean aperture and surface roughness. Our results were in good agreement with previous studies on two-dimensional fractures. We found a clear relationship between permeability and mean aperture. Both in uniform and non-uniform geometry have the same trend as the mean aperture increased, permeability generally increased, while rougher surface roughness permeability generally decreased but in non-uniform geometry the data on the graph appears more random and irregular. We extended our investigation to real fractures by digital rock portal data. The analysis revealed that the geometry of the real fractures closely resembled non-uniform geometry, and the permeability exhibited anisotropic behaviour. In addition, the anisotropy of permeability and computation time were also investigated; and it was found that both can be influenced by the three-dimensional fracture geometry.

1. Introduction

A petroleum reservoir is a subsurface rock structure that is formed naturally due to tectonic activity, and consists of pores and fracture networks [1,2]. Some of the hydrocarbon reservoirs in Indonesia are characterised by a fractured form. Herdiansyah *et al.,* [3] also noted that in Indonesia, volcaniclastic reservoirs that exhibit significant production are highly dependent on natural fractures, which play a critical role in determining the reservoir's quality and quantity; for instance, they

*Corresponding author.
E-mail: iad@geophys.unpad.ac.id (Irwan Ary Dharmawan)

https://doi.org/10.37934/cfdl.15.12.118

enhance fluid flow and transport of fluids [4,5]. Fractures may present as simple linear features; however, in fracture media, the geometric shapes are more complex and irregular [6-9]. This is because the fracture has surface roughness and a variable mean aperture. Mean aperture refers to the average width of the fracture's gap, and surface roughness measures the level of irregularity on the fracture surface, which thus affects geometric shape [6].

The irregular geometric shape of the fracture surface is another major factor affecting the characteristics and mobility of fluid flows in the fracture geometry [7, 10-12]. Previous studies have shown that the irregularity of fractures can significantly impact fluid flow. For example, Dhou and Zhou [13] studied solute transport in a single rough fracture with two-dimensional (2-D) geometry. Dharmawan *et al.,* [14] conducted a simulation study on the flow of non-Newtonian fluids in a two-dimensional fracture network, with a finite Reynolds number, in order to numerically analyse the flow velocity, shear stress and viscosity, and investigate their dependence on the fluid rheology and the effects of fracture geometry. Wang *et al.,* [15] conducted numerical simulations of three-dimensional (3-D) single-phase flow through self-affine fracture models and found that surface roughness can affect the transmissivity, hydraulic aperture, and tortuosity of flow paths. Zhang *et al.,* [16] presented a 3D microscale flow simulation of both Newtonian and cross power-law shear-thinning fluids through a realistic rough fracture, to evaluate the critical Reynolds number beyond which the linear Darcy's law was no longer applicable, and they quantified the simulated velocity fields. Additionally, Tian *et al.,* [17] investigated the influence of fracture geometry on the nonlinear fluid flow behaviour in rough fractures; they found that nonlinearity depends on several factors, including aperture, element size distribution standard deviation, driving pressure gradient, and fracture tortuosity. These studies collectively indicate that the irregularity of fractures can significantly affect fluid flow behaviour.

Every reservoir rock has the capacity to allow fluid to pass through it, which is referred to as permeability. It is a key physical property that is essential for understanding the behaviour of subsurface reservoirs, because it plays a critical role in determining the efficiency of fluid recovery from reservoirs, including oil and gas. In the case of fractures, due to variations in mean aperture, surface roughness, and orientation of fractures, it is important to calculate their permeability, because it can greatly enhance the permeability of rocks and significantly impact fluid flow. Recently, Irayani *et al.,* [18] calculated the permeability of different types of sandstone rocks using 3D tomographic images. Furthermore, the study aimed to determine the degree of anisotropy in permeability based on flow direction; the results indicate that permeability is slightly anisotropic. Rezaei Niya and Selvadurai [19] examined the relationship between the Joint Roughness Coefficient (JRC) and permeability of a 3-D fracture through a numerical study based on COMSOL multiphysics. However, this study has several limitations. For instance, Yin *et al.,* [20] found that the JRC cannot reflect the realistic influence of roughness on the permeability of a single fracture, and the numerical method used has some drawbacks, such as difficulties in dealing with complex boundary conditions for conventional numerical models and it is known that conventional numerical methods discretize the macroscopic equations. However, LBM is based on simplified kinetic models integrating physics of microscopic processes where macroscopic properties obey the desired equations [21]. To address these issues, Yin *et al.,* [20] conducted a similar study using the Lattice Boltzmann Method, to investigate the fluid flow behaviour through rough fractures on a 2-D profile fracture geometry. The Lattice Boltzmann Method (LBM) is a numerical method that uses a mesoscopic approach to describe fluid dynamics processes with complex boundary conditions, such as those found in porous media that can describes and captures physics better [22-24]. The LBM method has several advantages, including a simple algorithm, efficiency on parallel systems, and suitability for dealing with complex geometries and boundary conditions [24-26]. However, two-dimensional geometry is less

representative of realistic rock conditions. Three-dimensional models provide a more realistic representation of the complex structure and connectivity of natural rock formations; this can more accurately capture the the formations complex geometry and the flow patterns of fluids through them, and thus significantly affect fluid flow behaviour [27]. Therefore, this study was conducted to gain a deeper understanding of the effect of geometry on permeability estimation in 3D fractures using the Lattice Boltzmann Method.

2. Methodology

The method used in this study consists of several steps. First, a three-dimensional fracture geometry was generated using fractal Brownian motion (fBm) through SmartFract software [28]. Next, the geometry was inputted into the LBM program; input parameters were set to read the geometry, and also to determine pressure conditions at the inlet and outlet. Then, numerical simulations were performed using the Lattice Boltzmann Method to calculate the permeability of the three-dimensional fracture geometry. Finally, the results are presented in the form of permeability graphs against surface roughness, based on variations in mean aperture. Overall, the research flow in this study is shown in Figure 1.

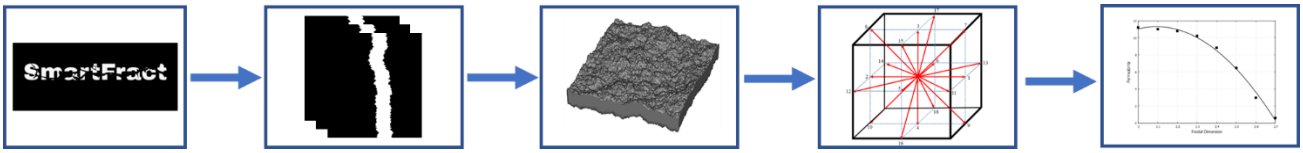

Fig. 1. The Flow of this study

In this study, the three-dimensional fracture geometries were created synthetically using SmartFract software [28]. Fractional Brownian motion, proposed by Madadi *et al.,* [29], was applied in this software to form roughness on the fracture surface based on the Hurst exponent value. Eq. (1) represents a calculation related to the Hurst exponent (H) and the fractal behaviour of a surface or signal.

$$\langle [B_H(\boldsymbol{r}) - B_H(\boldsymbol{r}_0)]^2 \rangle \sim |\boldsymbol{r} - \boldsymbol{r}_0|^{2H} \tag{1}$$

$B_H(\boldsymbol{r})$ and $B_H(\boldsymbol{r}_0)$ provide the values of the surface or signal measured at two different points, $\boldsymbol{r}$ and $\boldsymbol{r}_0$, while the distance between these points is represented by $|\boldsymbol{r} - \boldsymbol{r}_0|$. When $H > \frac{1}{2}$, fBm shows persistence or a positive correlation. The high or low altitude of $\boldsymbol{r}$ is reflected in by a similar trend at $\boldsymbol{r} + \Delta\boldsymbol{r}$. In contrast, when $H < \frac{1}{2}$, fBm resulted in anti-persistence or negative correlation. The magnitude of the height at r will result in the opposite height at $\boldsymbol{r} + \Delta\boldsymbol{r}$.

The roughness of the fracture surface is captured by the Hurst exponent (H) in the value range $0 < H < 1$. A greater value of H indicates a smoother fracture surface, while a smaller value denotes a rougher surface. In three-dimensional fracture geometry [5], the relationship between the fractal dimension (D) and Hurst exponent (H) can be expressed in Eq. (2):

$$D = 3 - H \tag{2}$$

This relationship is based on the observation that the Hurst exponent is related to the self-similarity of a fractal object, and the fractal dimension refers to the roughness or complexity of a fractal object.

In this study, we adopted the model described by Sahimi *et al.,* [6], where fractures were initially represented by a 3D channel between two parallel flat surfaces. The self-affine roughness profile was then generated and superimposed on top of the flat surfaces. The geometry used was $200 \times 200 \times 200$ in size, with the flow in the $\boldsymbol{x}$ and $\boldsymbol{z}$ directions. The fracture geometries used consist of uniform and non-uniform geometries, with Hurst exponent (H) values ranging from 1 to 0.3; this resulted in fractal dimensions in the range of 2 to 2.7, which describe the surface roughness conditions from smoothest to roughest. This variation is observed because the Hurst exponent of natural rock fractures has been found to mainly vary between 0.45 and 0.85, which corresponds to a 3D fractal dimension between 2.55 and 2.15 [15, 30-32]. In reference to the real fracture study conducted by Karpyn *et al.,* [33] that used a length of 800 lattice units, which represents approximately 101.42 mm. Based on this conversion, the length of the fracture in our geometry is estimated to be around 25.35 mm.

Figure 2 shows the differences between geometry uniform and non-uniform. Geometry uniform fractures were defined as those in which the surface roughness at the top and bottom sections was identical because the roughness profile from the top surface is directly copied and applied to the bottom surface ensuring a consistent roughness profile and aperture throughout the fracture. However, the geometry of non-uniform fracture geometry exhibited distinct surface roughness values between the top and bottom of surface creating variations in the roughness characteristics and the aperture along the fracture length. The mean aperture of fractures varied from 10 to 30 lattice units (lu), representing narrow to wide fracture gaps. Every voxel is given a value 0 for a fluid or pore voxel and 1 for a material voxel.

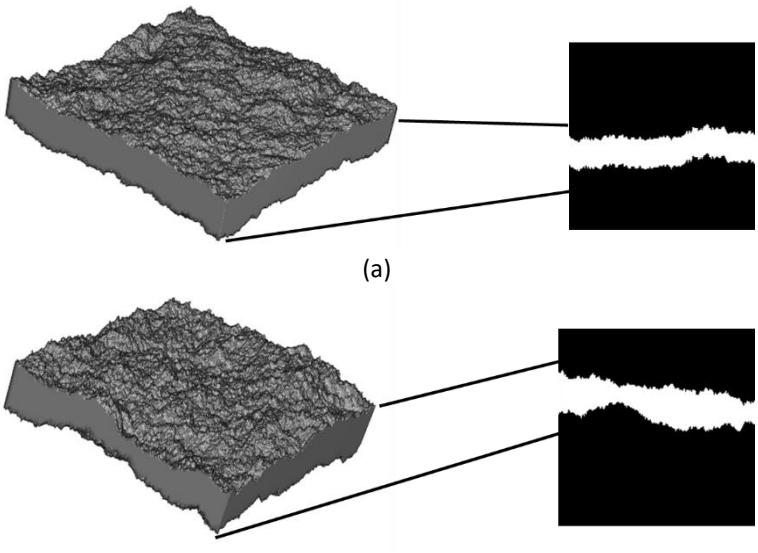

(a)

(b)

Fig. 2. Three-dimensional fracture with $H = 0.5$ and mean aperture 20 lu for (a) uniform geometry and (b) non-uniform geometry

The Palabos program with the Lattice Boltzmann numerical approach, developed by Jonas Latt *et al.,* [34], was used in this study. The next step was to create an input file from the images, so that the code could read in the geometry. The resulting three-dimensional geometric shape was then sliced in the $\boldsymbol{x}$ direction to obtain a collection of two-dimensional binary image files; thus 200 binary images (*.bmp*) were formed with a size of 200×200. The geometric parameter input was set using a function in Matlab that was already available in Palabos, in order to stack the collection of binary

images to form a 3D fracture geometry that could be input to the Palabos program in the form of a *.dat* file. The geometry was set by the input of the following program to establish the boundary conditions for this simulation. The geometry or material was set as a bounce back, and the inlet and outlet were given a fixed pressure difference of 5×10^{-5}, defined as constant pressure at the inlet and a constant lower pressure at the outlet. The fluid initially had zero velocity, with a linear pressure gradient along the flow direction. To check the Reynolds number (Re) used in our simulation, we utilized the formula provided in Eq. (3).

$$Re = (\frac{\rho v L}{\mu}) \tag{3}$$

By considering the fluid density to be 1 or less, the average velocity obtained from the simulation is within the range of 10^{-6}. With a flow path length of 200 and a viscosity value of 1.67, we calculated the Reynolds number (Re) to be 0.1198. With the given Reynolds number, this fluid flow is already classified as creeping flow.

Furthermore, to validate our findings and establish a connection with real rock scenarios, we incorporated data from the Digital Rock Portal, specifically the micro-CT rough fracture in Berea sandstone-core dataset [33]. The real fractures in this dataset have a mean aperture of 18.6 lu and $H = 0.6$. We refer to the profile of the mean distribution of real fractures, as investigated by Zhang *et al.,* [16], which reveals that the mean aperture distribution is variated. This dataset comprises real fracture geometries observed in natural rock formations, which often exhibit non-uniform characteristics. Figure 3 shows the original fracture, which has a size of $800 \times 800 \times 220$. It was converted to a binary matrix representation and then divided into four equal sub-samples, each with dimensions of $200 \times 200 \times 220$ using MATLAB. This was done by selecting specific ranges from the original matrix. The four sub-samples were named A, B, C, and D. This resampling process allowed for more focused analysis and examination of the fracture characteristics within smaller, yet representative, portions of the original dataset. Permeability and anisotropy were calculated for the resampled fractures. By analysing the permeability and anisotropy based on these real fracture geometries, we aimed to enhance the relevance and applicability of our study to real-world scenarios.

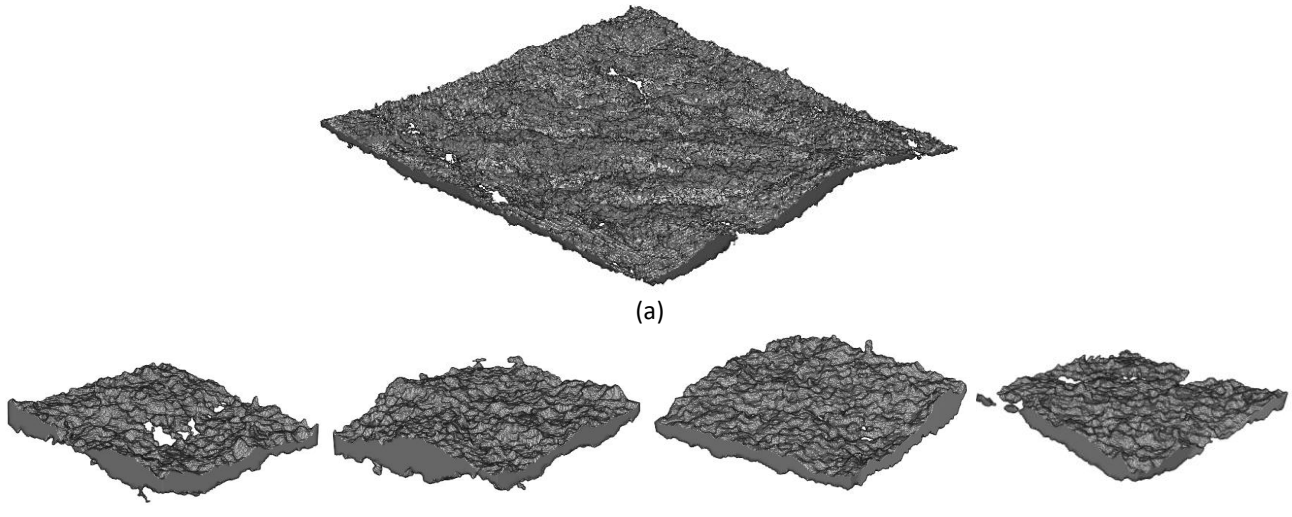

Fig. 3. Three-dimensional real fracture geometry with mean aperture 18.6 lu with $H = 0.6$, (a) original fracture with size $800 \times 800 \times 220$, and resampling fracture (b) sample A, (c) sample B, (d) sample C, and (e) sample D with size $200 \times 200 \times 220$

The LBM method used in this study involved a mesoscopic approach, which means that the collective properties of multiple particles were viewed as a quantity defined by a distribution function $f(\boldsymbol{x}, \boldsymbol{c}, t)$. Particles behaviour are pre-averaged or only particle distributions that live on the lattice nodes are traced, rather than all the individual particles [35]. This distribution function represents the density values of the existing particles, with f_i being a continuous distribution function at the i-th point, as a discrete variable that is a function of velocity ($\boldsymbol{c}$) at position ($\boldsymbol{x}$) and time (t), as shown in Eq. (4).

$$\rho(\boldsymbol{x}, t) = \sum_i f_i(\boldsymbol{x}, t) \tag{4}$$

The LBM method discretised the velocity ($\boldsymbol{c}_i$); time (Δt), which was the time step; and position (Δx), which was the distance between the lattices, with Δx and Δt indicating the resolution of the lattice units. The discretisation of velocity depended on the $\mathrm{D_nQ_m}$ model used, and the simulation used the $\mathrm{D_3Q_{19}}$ model, which had a three-dimensional shape with 19 discrete velocity directions or particle movement directions, as shown in Figure 4 below. By discretising the Boltzmann equation in velocity, space and time, the Boltzmann equation can be written as Eq. (5) [36],

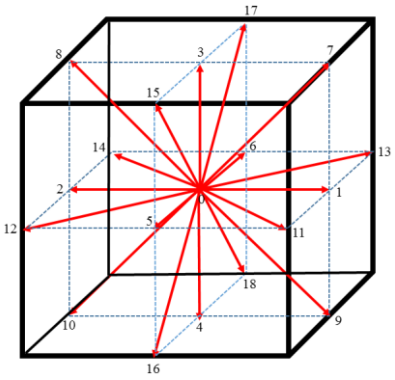

Fig. 4. Illustration of D3Q19 Model

$$f_i(\boldsymbol{x} + \boldsymbol{c}_i \Delta t, t + \Delta t = f_i(\boldsymbol{x}, t) + \Omega_i(f) \tag{5}$$

where the density distribution function $f_i(\boldsymbol{x}, t)$ represents the density values moving in the i-th direction with velocity $\boldsymbol{c}_i$ towards its nearest point $\boldsymbol{x} + \boldsymbol{c}_i \Delta t$ at time $t + \Delta t$. The particles also experienced collisions with each other, affected by the collision operator $\Omega_i(f)$. The simulation used the Bhatnagar Gross Krook (BGK) approach, which described the process of the distribution function's relaxation towards equilibrium (f_i^{eq}) with a relaxation time τ, as mathematically expressed in Eq. (6).

$$\Omega_i(f) = -\frac{f_i - f_i^{eq}}{\tau} \Delta t \tag{6}$$

The equilibrium distribution function is represented in Eq. (7), where c_s is the sound speed, $\boldsymbol{c}_i$ are the discrete velocities, and w_i are weights [36]. The macroscopic density is represented by ρ and the macroscopic velocity vector is represented by $\boldsymbol{u}$.

$$f_i^{eq}(\boldsymbol{x}, t) = w_i \rho \left[1 + \frac{\boldsymbol{c}_i \cdot \boldsymbol{u}}{c_s^2} + \frac{(\boldsymbol{c}_i \cdot \boldsymbol{u})^2}{2c_s^4} - \frac{(\boldsymbol{u})^2}{2c_s^2}\right] \tag{7}$$

The weight factor for each of the velocity links, as shown in Figure 4, is presented in Table 1.

Table 1
The weighting coefficients for $\mathrm{D_3Q_{19}}$ model

Model	$\boldsymbol{w_i}$
$\mathrm{D_3Q_{19}}$	$\frac{1}{3}\ (i=0)$
	$\frac{1}{18}\ (i=1,\dots,6)$
	$\frac{1}{36}\ (i=7,\dots,18)$

The particle distribution function in each time iteration was calculated using the Bhatnagar Gross Krook (BGK) approximation, which involved two main steps: collision and streaming. The distribution function changed due to the collision operator, and then it was streamed to the nearest point. Furthermore, the Lattice Boltzmann equation with the BGK collision operator can be expressed as Eq. (8).

$$f_i(\boldsymbol{x}+\boldsymbol{c}_i\Delta t, t+\Delta t) = f_i(\boldsymbol{x},t) - \frac{\Delta t}{\tau}(f_i(\boldsymbol{x},t) - f_i^{eq}(\boldsymbol{x},t)) \tag{8}$$

The macroscopic values such as fluid density and momentum are obtained by summing the distribution functions, as shown in Eq. (9) and Eq. (10).

$$\rho = \sum_i f_i \tag{9}$$

$$\rho\boldsymbol{u} = \sum_i \boldsymbol{c}_i f_i \tag{10}$$

Darcy's law, a basic concept in fluid mechanics that describes fluid flow through porous media, was used to calculate the permeability of three-dimensional fractures in this study. While the cubic law is commonly applied for calculating flow within fractures characterized by smooth and flat surfaces separated by a constant aperture [17]. However, the fractures considered in our study exhibit surface roughness, and their intricate geometries were captured and represented numerically. Due to the complexity of our fracture geometry and the presence of surface roughness, the Darcy equation was chosen as the appropriate method for permeability calculations. Unlike the cubic law, which assumes parallel plates and a constant gap, the Darcy equation accommodates the consideration of complex geometries and surface roughness effects.

The rate of fluid flow through porous media was proportional to the pressure gradient across the media, and the constant of proportionality was known as the permeability coefficient, which was a measure of the medium's ability to conduct fluid. The flow rate, pressure gradient, and permeability coefficient are related mathematically in Eq. (11),

$$Q = -\frac{kA}{\mu}\nabla P \tag{11}$$

where Q is the flow rate, k is the permeability, A is the cross-sectional area of the medium, and ∇P represents the pressure gradient. The numerical simulation of the three-dimensional fracture geometry enabled the calculation of permeability using Darcy's law.

3. Results

The geometries were generated with varying roughness and aperture sizes. Figure 5 shows the resulting 3D uniform and non-uniform geometries for H values of 0.3, 0.6, and 0.8, with 10, 20, and 30 lu (lattice unit) as the mean aperture. When the H value increases, the geometries become rougher and more complex, with greater irregularities and variations in the aperture size. Similarly, as the aperture size increases, the geometries become wider and more open, with larger variations in the aperture size. These differences in the geometry can have a significant impact on the resulting fluid flow behaviour, as described in the following sections. As we can see the differences between the uniform and non-uniform geometries the roughness profile is the same at the top and bottom, so the aperture is constant throughout. In non-uniform fractures, the roughness profile is different at the top and bottom, so the aperture varies.

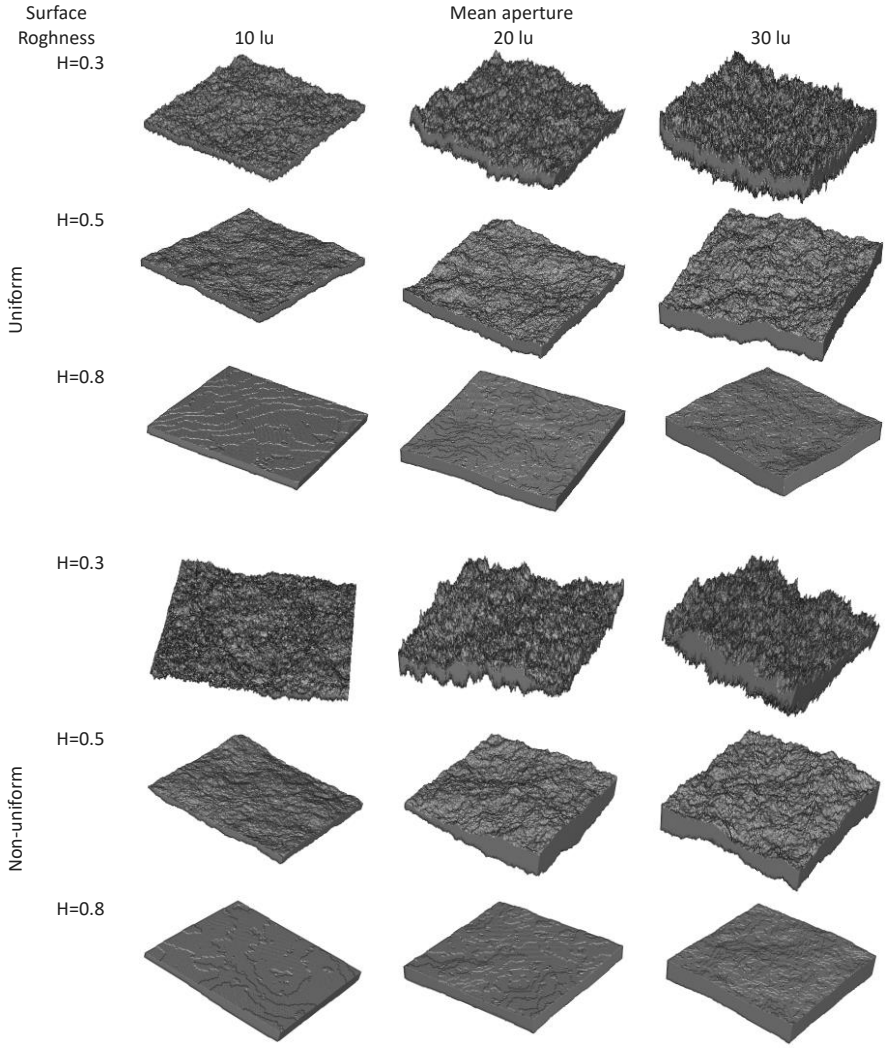

Fig. 5. Three-dimensional fracture uniform and non-uniform geometry with various mean aperture from 10-30 lu with $H = 0.3,\ H = 0.5$, and $H = 0.8$

Validation of Poiseuille Flow was conducted to ensure that the simulation program used could accurately simulate fluid flow velocity. This validation was carried out using a parallel plate geometry through which an incompressible fluid with viscosity flowed in a laminar flow. Poiseuille Flow can be used to validate the flow by comparing the velocity profile obtained analytically with the results

obtained from numerical simulation. The results, shown in Figure 6(a), indicate that the velocity profiles obtained analytically and numerically have a similar general shape. To confirm the difference, the Root Mean Square Error (RMSE) was calculated, resulting in an RMSE value of 0.0052. This indicates good agreement between the analytical and numerical values, demonstrating that the program can accurately simulate fluid flow velocity. The convergence of mesh has been studied in this research using various numbers of grid points, which impacts the resolution of the simulation. It refers to the phenomenon where using finer or more grids lead to numerical calculations approaching the exact or desired values. Multiples of 2^n are used to ensure an exponential increase in the number of grids. This allows for systematic comparison of the effects of different grid numbers. The grid numbers used are multiples of 2^n, starting from 32, 64, 128, 256, 512. Based on the graph in Figure 6(b), it can be observed that using fewer grids to capture the geometric surface shape, resulting in lower numerical accuracy. From 128 to 512 grids, the graph shows stability with numerical calculations that are not significantly different from each other, approaching the exact values better than the previous grid numbers. Additionally, finer grids were employed in this study to further enhance the precision of our calculations.

The LBM assumes incompressible flow to solve the Navier-Stokes equations. This simulation is valid when the lattice velocity is significantly lower than the speed of sound in the lattice, indicating a low Mach number condition [37,38]. It is crucial to limit the lattice velocity to be below approximately 0.1 lu ts^{-1} [37]. This limitation is a result of the low Mach number assumption, which allows LBM to accurately simulate hydrodynamics. In this study, the average lattice velocity falls within the range of 10^{-6} to 10^{-8} lu ts^{-1}, indicating that it is much smaller than the threshold of 0.1 lu ts^{-1}. This suggests that the lattice velocity is within an acceptable range to maintain the low Mach number approximation in LBM simulations. Therefore, it can be considered appropriate to satisfy the requirement for accurately simulating hydrodynamics using the low Mach number approximation in LBM.

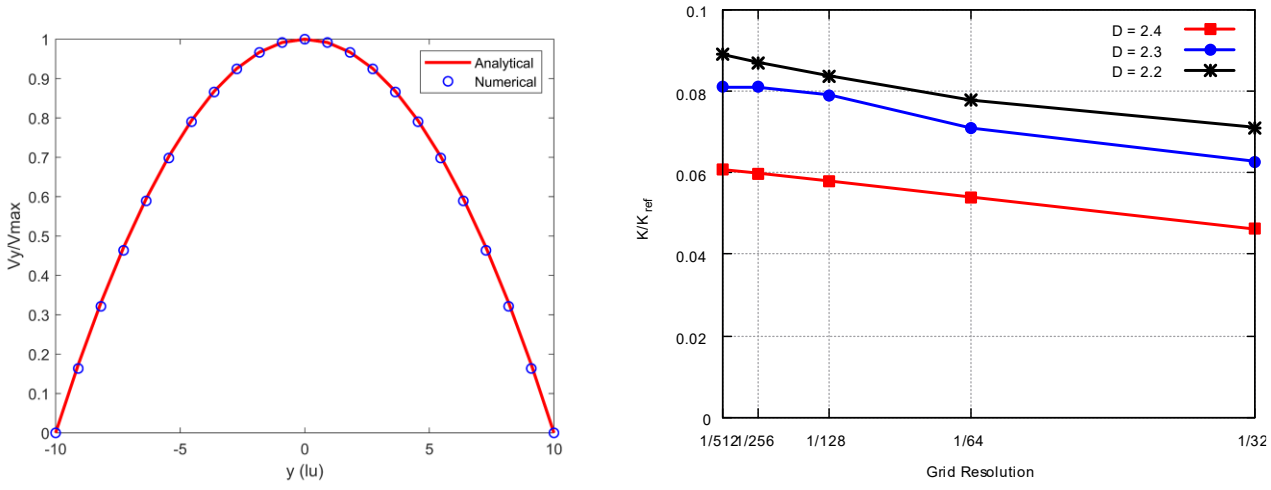

(a) (b)

Fig. 6. Validation of (a) Poiseuille flow velocity profile and (b) Mesh Convergence

In this study, to analyze the velocity distribution, a specific z-coordinate ($\boldsymbol{z} = 20$) was selected to compare velocities across different surface roughness levels, ranging from rough to smooth surface. Velocities were calculated and normalized based on the smoothest fracture surface, allowing for relative comparisons. Figure 7 visually represents the velocity profiles for different surface roughness levels. The colors used in the figure indicate velocity levels, with red representing the highest velocities and dark blue indicating the lowest. This visualization helps to understand the variation in

velocity across the flow domain. The results of the study revealed certain trends. Regardless of the surface roughness level, the velocities were observed to be relatively low at the edge of the flow near the fracture surface. This can be attributed to the presence of surface irregularities and roughness, which disrupt the smooth flow of the fluid and create resistance. In contrast, higher velocities were found in the central region of the flow. This can be explained by the fact that the fluid encounters less resistance as it moves away from the rough fracture surfaces towards the center of the fracture. The smoother regions within the fracture allow for more streamlined flow, resulting in higher velocities.

The study analysed the different surface roughness levels by observing the velocity profiles. The roughest surfaces ($H = 0.3$) displayed predominantly blue in the velocity profile, indicating the lowest velocity distribution. As the surface roughness decreased ($H = 0.5$), the velocity increased and was represented by blue and green colors. Further decreasing surface roughness ($H = 0.6$) led to an even higher velocity, with the appearance of yellow in the middle of the flow. The highest velocities were observed at the smoothest surface conditions ($H = 0.8$ and $H = 1.0$), represented by the color red. These findings highlight the significant influence of surface roughness on the velocity distribution within fracture flow at the pore scale. The roughness of the fracture surface directly affects the flow behaviour, with rougher surfaces leading to lower velocity distributions. The complex and irregular nature of rough surfaces introduces additional resistance and turbulence to the flow, resulting in reduced velocities. Understanding the impact of surface roughness on velocity distribution in fracture flow is crucial for comprehending fluid transport in fractures. It provides valuable insights into fluid behaviour at small scales and enhances our understanding of flow dynamics within fractures, with potential applications in areas such as hydrocarbon recovery, groundwater flow, and subsurface geology.

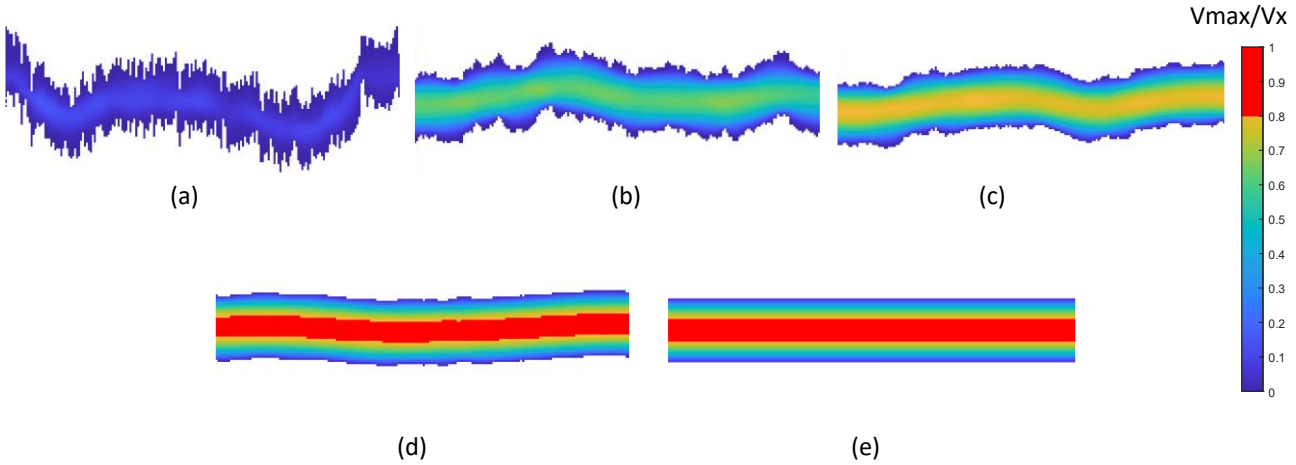

Fig. 7. Normalised velocity profile for various surface roughness on XY Plane, (a) $H = 0.3$, (b) $H = 0.5$, (c) $H = 0.6$, (d) $H = 0.8$, and (e) $H = 1.0$

Table 2 shows permeability values in both $\boldsymbol{x}$ and $\boldsymbol{z}$ flow directions, for various mean aperture and surface roughness values. In this study, normalized permeability values with respect to K_{ref} are used. The value of K_{ref} used is 11.2126, representing the maximum permeability obtained for two parallel smooth plates and with a mean aperture of 30 lu. Anisotropy of permeability values was also calculated to indicate the effect of changes in fracture orientation or direction on fluid flow. The anisotropy values were generally around 1, indicating isotropic behaviour. However, if the values deviated significantly from 1, it would indicate anisotropic behaviour. The phenomenon of non-uniform geometry can also be observed in real fractures. This can be seen in the distinct roughness profiles at the top and bottom surfaces of the fracture. In this study, both the permeability and

anisotropy of permeability were calculated for real fractures in the resampled size. The results are presented in Table 2. The findings indicate that the anisotropy values deviate from 1, suggesting an anisotropic behaviour in these real fractures, similar to what is observed in non-uniform geometries. This observation further supports the notion that real fractures exhibit characteristics to non-uniform geometries.

Additionally, the results in Table 2 and Figure 8 also show the mean aperture's crucial role in determining permeability of the fracture. The permeability generally increased with mean aperture due to the greater space available for fluid flow both in uniform geometry and non-uniform geometry. It has been found that there is a pattern in both cases where, for larger Fractal Dimension values indicating a rough surface ($D = 2.6$ and $D = 2.7$), the relationship between mean aperture and permeability becomes linear based on the graph, which shows a linear increase as the mean aperture of the fracture increases. As the surface becomes smoother, the graph becomes nonlinear that the graph increasing exponentially. There is also a slight difference observed between the uniform and non-uniform graphs. In Figure 8(a) and Figure 8(b) the lines in the uniform graph are arranged in order from the highest Fractal Dimension to the lowest, corresponding to the lowest permeability to the highest permeability. In the other hand, in the non-uniform geometry (Figure 8(c-d)) the graph appears random and not in any particular order, unlike the orderly pattern observed in the uniform geometry graph. This difference arises due to the varying and diverse aperture that present in the non-uniform geometry, resulting from different surface roughness profiles on its upper and lower parts. This is in contrast to the uniform geometry where the upper and lower parts are identical, resulting in a uniform and consistent aperture width at every point.

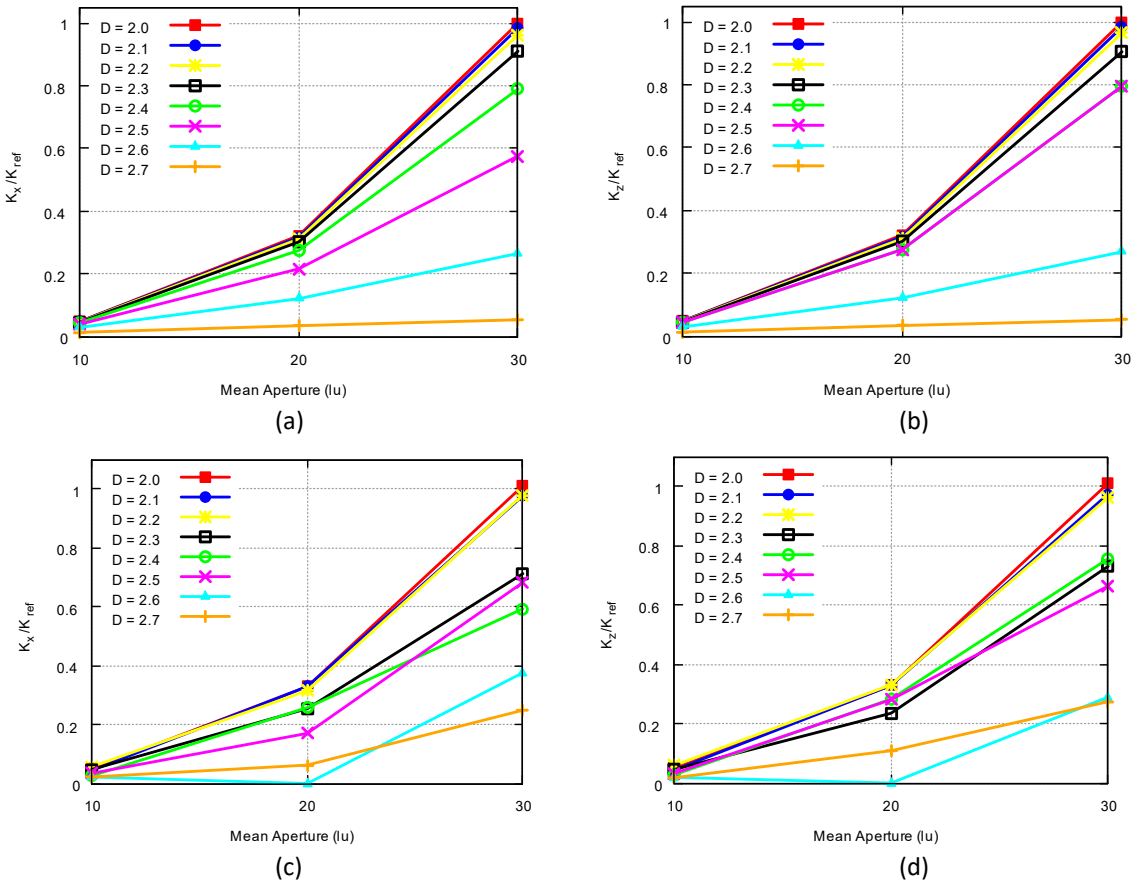

Fig. 8. Effect of mean aperture on permeability of single fractures in (a) $\boldsymbol{x}$-direction, (b) $\boldsymbol{z}$-direction flow on uniform geometry and (c) $\boldsymbol{x}$-direction, and (d) $\boldsymbol{z}$-direction flow on non-uniform geometry

Table 2
Permeability values for real fracture, uniform and non-uniform three-dimensional fractures with different mean apertures and surface roughness in flow in the x-Direction and z-Direction

Mean Aperture (lu)	H	D	Uniform fracture Geometry			Non-Uniform fracture geometry		
			Permeability x-Direction (K_x/K_{ref})	Permeability z-Direction ($K_z//K_{ref}$)	Aniso-tropy	Permeability x-Direction (K_x/K_{ref})	Permeability z-Direction ($K_z//K_{ref}$)	Aniso-tropy
10	1	2	0.048	0.048	1.000	0.049	0.049	1.000
	0.9	2.1	0.047	0.047	1.000	0.044	0.044	1.015
	0.8	2.2	0.047	0.047	1.001	0.057	0.059	0.969
	0.7	2.3	0.046	0.046	1.000	0.048	0.045	1.059
	0.6	2.4	0.044	0.044	1.002	0.026	0.027	0.950
	0.5	2.5	0.039	0.039	1.006	0.035	0.032	1.075
	0.4	2.6	0.029	0.029	1.001	0.022	0.019	1.167
	0.3	2.7	0.013	0.013	1.009	0.022	0.018	1.224
20	1	2	0.322	0.322	1.000	0.329	0.329	1.000
	0.9	2.1	0.316	0.316	1.000	0.330	0.329	1.000
	0.8	2.2	0.311	0.310	1.002	0.315	0.332	0.950
	0.7	2.3	0.302	0.302	1.001	0.255	0.236	1.081
	0.6	2.4	0.275	0.275	0.998	0.258	0.283	0.910
	0.5	2.5	0.216	0.214	1.013	0.170	0.281	0.605
	0.4	2.6	0.121	0.122	0.992	0.196	0.182	1.076
	0.3	2.7	0.035	0.034	1.027	0.063	0.109	0.574
30	1	2	0.999	0.999	1.000	1.011	1.011	1.000
	0.9	2.1	0.983	0.983	1.000	0.977	0.975	1.002
	0.8	2.2	0.962	0.964	0.998	0.980	0.964	1.017
	0.7	2.3	0.910	0.905	1.005	0.713	0.731	0.975
	0.6	2.4	0.789	0.795	0.993	0.594	0.757	0.784
	0.5	2.5	0.576	0.568	1.015	0.683	0.665	1.027
	0.4	2.6	0.265	0.268	0.988	0.377	0.290	1.298
	0.3	2.7	0.053	0.051	1.039	0.249	0.274	0.908
Real_A	0.6	2.4				0.041	0.008	5.352
Real_B						0.095	0.071	1.333
Real_C						0.061	0.037	1.662
Real_D						0.013	0.008	1.601

The permeability is calculated for different surface roughness described by fractal dimensions at different apertures, as illustrated in Figure 9(a-c) for x-direction flow and Figure 9(d-f) for z-direction flow in uniform fracture geometry meanwhile in Figure 10(a-c) for x-direction flow and Figure 10(d-f) for z-direction flow in non-uniform fracture geometry. The red line represents the permeability values for a mean aperture of 10 lu, the blue line for a mean aperture of 20 lu, and the black line for a mean aperture of 30 lu. The horizontal axis represents the fractal dimension, while the vertical axis shows represents the normalized permeability values with respect to K_{ref}. Regarding the relationship between surface roughness and permeability, it can be seen that the permeability of the fractures decreases as the fractal dimension increases, both in x-direction flow and z-direction flow. This means that the rougher the fracture surface, the lower the permeability value. The results are in agreement with the findings from a two-dimensional single fracture obtained by Yin *et al.,* [20].

Smoother fracture surfaces have a higher Hurst exponent or lower fractal dimension, which the flow paths through the fractures tend to be more direct and less tortuous. This is because the smoother surfaces offer less resistance to fluid flow, resulting in higher permeability. The fluid can easily flow through the wider portions of the fractures, which also contributes to the increased

permeability. However, when the fracture surfaces are rougher, with a lower Hurst exponent or higher fractal dimension, the flow paths become more convoluted and tortuous, because the rough surfaces create more obstructions and irregularities, which hinder fluid flow and increase the resistance. The fluid encounters narrower and more restricted flow paths within the fractures, leading to decreased permeability. In both the uniform and non-uniform graphs, a similar trend can be observed where the permeability decreases as the fractal dimension increases. However, there are differences between the two. In the uniform geometry, as depicted in Figure 9, the data is neatly arranged and follows the expected trend. In contrast, in the non-uniform geometry shown in Figure 10, the data on the graph appears more random and irregular. This is because the non-uniform geometry incorporates different surface roughness profiles in its upper and lower parts, resulting in a more complex and irregular geometry compared to the uniform geometry.

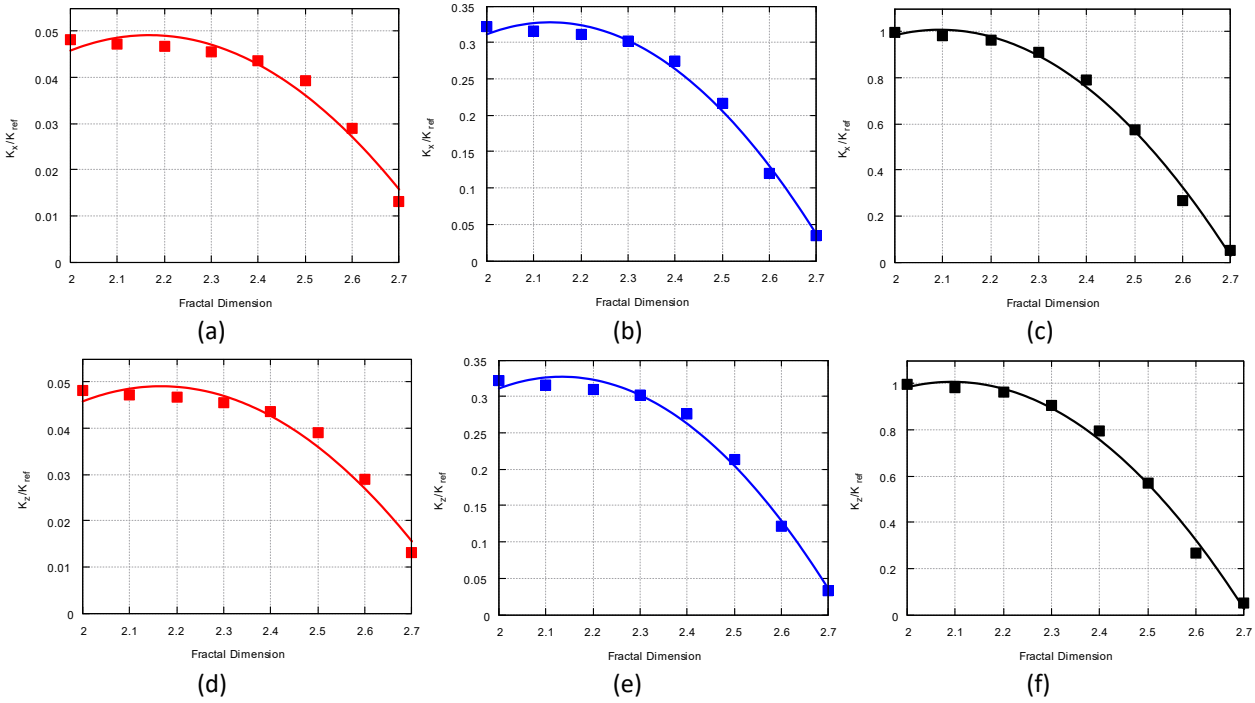

Fig. 9. Effect of fractal dimension on permeability of uniform geometry single fractures with apertures (a) 10 lu, (b) 20 lu, (c) 30 lu in x-direction flow and (d) 10 lu, (e) 20 lu, (f) 30 lu in z-direction flow

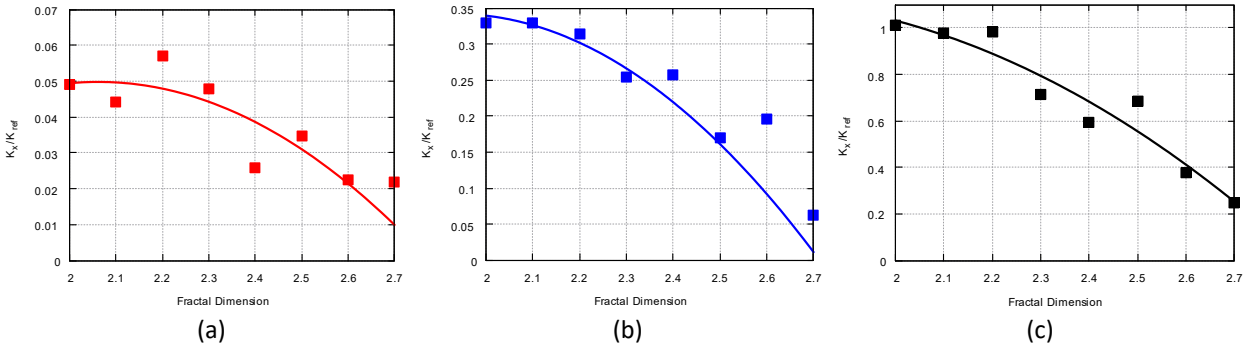

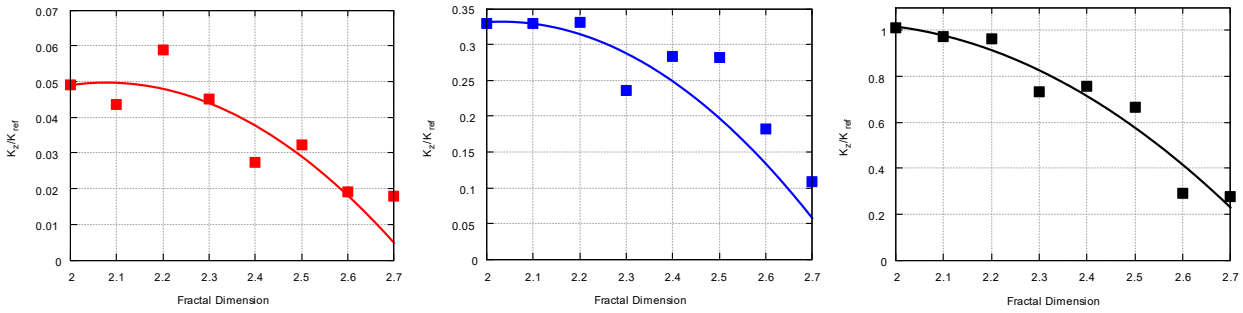

(d) (e) (f)

Fig. 10. Effect of fractal dimension on permeability of non-uniform geometry single fractures with apertures (a) 10 lu, (b) 20 lu, (c) 30 lu in $\boldsymbol{x}$-direction flow and (d) 10 lu, (e) 20 lu, (f) 30 lu in $\boldsymbol{z}$-direction flow

Further analysis was conducted to determine the influence of surface roughness on the anisotropy of permeability values. Figure 11 shows the anisotropy of permeability ($|\boldsymbol{kx}/\boldsymbol{kz}|$) for different surface roughness values at various mean apertures. The red line represents a mean aperture of 10 lu, the blue line indicates a mean aperture of 20 lu, and the black line shows a mean aperture of 30 lu, with the horizontal axis representing surface roughness and the vertical axis for the anisotropy of permeability values. The results show that when the fractal dimension is small, indicating smoother fracture surfaces, the anisotropy values become more stable and closer to 1, indicating isotropy. This is observed in $D = 2.0$ and $D = 2.1$, where the anisotropy values become more stable as they approach 1, especially at mean apertures of 10 and 20 lu. Then, at $D = 2.1$ and $D = 2.0$, all apertures have the same value of 1, indicating isotropy. In contrast, when the fractal dimension is greater, indicating rougher fracture surfaces, the anisotropy values move further away from 1, even reaching a maximum when the fracture surface is at its roughest ($D = 2.7$) and a minimum at $D = 2.6$. Fracture surfaces that are rougher in one direction than another can create preferential flow paths along the smoother surfaces. This can result in higher permeability in the direction parallel to the smoother surfaces than in the perpendicular direction and it made the anisotropy move further away from 1. Therefore, surface roughness has an effect on the anisotropy of permeability values, where smoother surfaces lead to values closer to isotropy.

Mean aperture was also examined for its influence on the anisotropy values. In Figure 11(a) for anisotropy of permeability in uniform geometry, it can be observed that as the mean aperture increases, the anisotropy values also increase. This is evident at $D = 2.7$, where the maximum anisotropy of a permeability value that is closest to 1 occurs at a mean aperture of 10 lu with a value of 1.01, while at a mean aperture of 30 lu, the value becomes greater and further away from 1, reaching 1.04. However, the non-uniform geometry exhibits a more anisotropic behaviour compared to the uniform fracture geometry. Figure 11(b) shows more fluctuating anisotropy values that deviate significantly from 1. For surface roughness with a Fractal Dimension of $D = 2.6$ and $D = 2.7$, the anisotropy values of permeability reach 1.3 and 0.5, respectively. The red line in the graph, representing a mean aperture of 10 lu, tends to be more stable and closer to 1, while the mean apertures of 20 lu and 30 lu tend to be more fluctuating, indicating a more anisotropic behaviour.

This result can be attributed to the different surface roughness profiles on the upper and lower parts, resulting in a more complex fracture geometry where the aperture widths are not uniform at every point. The different surface roughness profiles on the upper and lower parts of the fracture can be attributed to the anisotropic behaviour observed in 3D fractures with the same fractal dimension but varying mean aperture. This is because the interplay between flow obstruction and preferential flow paths is affected by the fracture geometry. Fractures are characterized by their

surface roughness, which contain localized barriers to fluid flow. These roughness elements act as obstacles, impeding the movement of fluid through the fracture. As fluid flows through the fracture, it tends to follow paths of least resistance. The presence of roughness elements creates variations in resistance along different pathways, leading to channeling effects. Channels with lower resistance, typically associated with regions of larger mean apertures, become favored pathways for fluid flow due to the lower resistance caused by roughness elements, resulting in a higher permeability. This preference for larger apertures accentuates permeability anisotropy as fluid movement becomes constrained in specific directions, resulting in an uneven distribution of flow within the fracture. Conversely, fractures with a constant mean aperture, despite having the same fractal dimension, exhibit more isotropic behaviour. In this case, the obstruction caused by roughness elements remains consistent throughout the fracture, promoting a balanced distribution of fluid flow in various directions, resulting in isotropy of flow within the fracture.

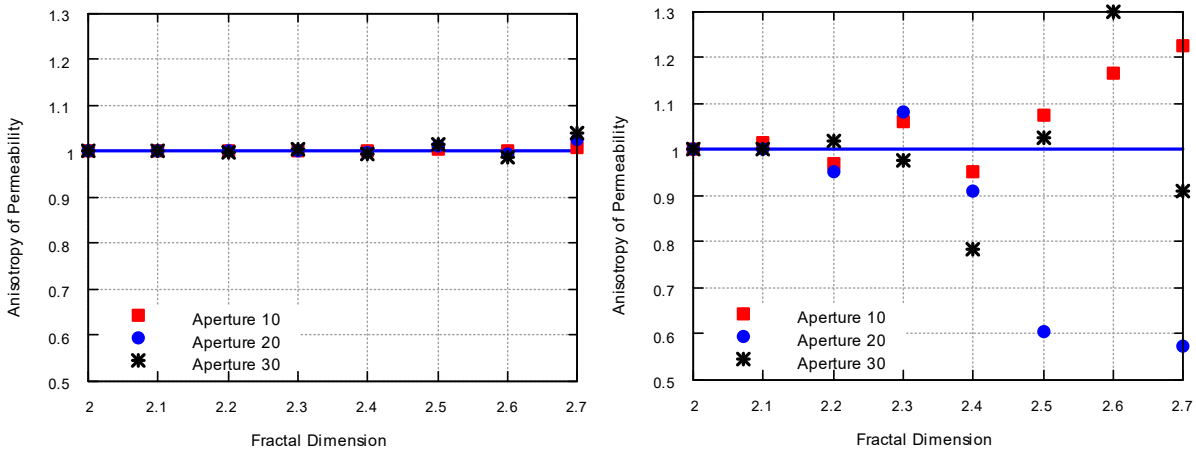

Fig. 11. Anisotropy of permeability ($|\boldsymbol{kx}/\boldsymbol{kz}|$) in different surface roughness described by the fractal dimension in (a) Uniform geometries and (b) Non-uniform geometries

Performing fluid flow simulation using LBM on complex geometries such as fractures usually requires longer computational time. The simulation stops when it reaches convergence, and can be performed using computers with a common specification. The required simulation time varies depending on the level of surface roughness and the number of cores used, as shown in Table 3, which compares the time consumption for simulations on a computer with Xeon® Gold 5118 CPU @2.30GHz processor specifications and 128 GB RAM, using different numbers of processors. A rougher surface results in higher complexity and longer time to reach convergence. The results indicate that for the roughest fracture surface ($D = 2.7$), it can take hours to reach convergence, while a smoother surface at $D = 2.4$ and $D = 2.1$ requires less time. Furthermore, increasing the number of cores used in parallel computing accelerates convergence and reduces the simulation time. However, it should be noted that for fractal dimension values greater than $D = 2.5$, the optimal and efficient number of cores to use is 16. This phenomenon may occur due to the increased coordination overhead between cores when using more than 16 cores, such as 32 cores, resulting in a longer simulation time.

Table 3
Comparison of time consumption for simulations with different numbers of CPU cores

Fractal Dimension	Mean Aperture (lu)	Number of Cores	Times
2.7	20	1	10H 35m 28s
		2	9H 17m 50s
		4	6H 56m 22s
		8	5H 14m 37s
		16	3H 30m 10s
		32	3H 10m 51s
2.4	20	1	15m 29s
		2	9m 30s
		4	6m 10s
		8	4m 11s
		16	4m 4s
		32	4m 20s
2.1	20	1	15m 18s
		2	9m 7s
		4	5m 32s
		8	4m 14s
		16	4m 4s
		32	4m 18s

4. Conclusions

In conclusion, our study highlights the significant influence of fracture geometry on fluid flow and permeability, and demonstrates the effectiveness of the Lattice Boltzmann Method in simulating these processes in complex three-dimensional fractures. Our findings indicate that geometric parameters of surface roughness and mean aperture can have a substantial impact on velocity distribution, permeability, and anisotropy of permeability. The complexity of the fracture surface roughness resulted in lower velocity distribution values for rougher surfaces. Furthermore, our results show that permeability decreases with an increasing fractal dimension, while it increases with an increase in mean aperture. These findings are consistent with those reported by Yin et al., [20] for two-dimensional single fractures. Both uniform and non-uniform fractures exhibit the same trend, but the data for non-uniform fractures is more irregular and random. This suggests that the fractal dimension is a more important factor for predicting permeability in non-uniform fractures. We also found that smoother surfaces lead to permeability values closer to isotropy, and as the mean aperture decreases, the anisotropy values become closer to 1, indicating a more isotropic behaviour. Our study reveals that uniform geometry, characterized by consistent surface roughness and mean aperture, exhibits isotropic behaviour in terms of permeability. In contrast, non-uniform geometry, with its varying surface roughness and mean aperture, displays anisotropic behaviour, indicating a directional dependency of permeability within the fracture. We also observed that the geometry of the real fractures closely resembled non-uniform geometry with anisotropic behaviour. Our study provides valuable insights into the relationship between fracture geometry and fluid flow, which can help in the development of accurate models for predicting fluid flow and permeability in geological formations.

Acknowledgement

The research was financially supported by the Hibah Kemdikbudristek Dikti 2023 scheme Penelitian Tesis Magister. The simulations were conducted on the "RockExplorer" cluster.

References

[1] Gunde, Akshay. "Spontaneous imbibition and solvent diffusion in fractured porous media by LBM." (2011). https://doi.org/10.7939/R3572K

[2] Guo, Boyun, Kai Sun, and Ali Ghalambor. *Well productivity handbook*. Elsevier, 2014. https://doi.org/10.1016/b978-1-933762-32-6.50010-7.

[3] Herdiansyah, Herdis, Habibullah Adi Negoro, Nurul Rusdayanti, and Siti Shara. "Palm oil plantation and cultivation: Prosperity and productivity of smallholders." *Open Agriculture* 5, no. 1 (2020): 617-630. https://doi.org/10.1515/opag-2020-0063

[4] Wynn, Tim. "Introduction to Naturally Fractured Reservoirs Part 1 – Fracture Origins, Characteristics and Parameters." *First Break* 40, no. 7 (2022): 31-40. https://doi.org/10.3997/1365-2397.fb2022054

[5] Askari, Amir Abbas, Golamreza Bashiri, and Mohammad Reza Kamali. "Model ranking and optimization of fractured reservoir using streamline simulation, case study a gas condensate reservoir." *In SPE Saudi Arabia Section Technical Symposium*. OnePetro, 2009. https://doi.org/10.2118/126074-MS

[6] Sahimi, Muhammad. *Flow and transport in porous media and fractured rock: from classical methods to modern approaches*. John Wiley & Sons, 2011. https://doi.org/10.1002/9783527636693

[7] Jing, Lanru, and Ove Stephansson. "The basics of fracture system characterization–Field mapping and stochastic simulations." In *Developments in geotechnical engineering*, vol. 85, pp. 147-177. Elsevier, 2007. https://doi.org/10.1016/S0165-1250(07)85005-X

[8] Chen, Tao, and Jean Borgomano. "The Impact of Fracture Geometries on Heterogeneity and Accuracy of Upscaled Equivalent Fracture Models*." Lithosphere 2022*, no. 1 (2022). https://doi.org/10.2113/2022/5070481

[9] Wang, Kang, Suping Peng, Yongxu Lu, and Xiaoqin Cui. "Wavefield simulation of fractured porous media and propagation characteristics analysis." *Geophysical Prospecting 70*, no. 5 (2022): 886-903. https://doi.org/10.1111/1365-2478.13198

[10] Zhao, Yan-long, Zhi-ming Wang, Jian-ping Ye, Han-sen Sun, and Jiao-yang Gu. "Lattice Boltzmann simulation of gas flow and permeability prediction in coal fracture networks." *Journal of Natural Gas Science and Engineering* 53 (2018): 153-162. https://doi.org/10.1016/j.jngse.2018.03.001

[11] Zhang, Yao, and Junrui Chai. "Effect of surface morphology on fluid flow in rough fractures: a review." *Journal of Natural Gas Science and Engineering* 79 (2020): 103343. https://doi.org/10.1016/j.jngse.2020.103343

[12] National Research Council. *Rock fractures and fluid flow: contemporary understanding and applications*. National Academies Press, 1996. https://doi.org/10.17226/2309

[13] Dou, Zhi, and Zhi-fang Zhou. "Lattice Boltzmann simulation of solute transport in a single rough fracture." *Water Science and Engineering* 7, no. 3 (2014): 277-287. https://doi.org/10.3882/j.issn.1674-2370.2014.03.004

[14] Dharmawan, I. A., R. Z. Ulhag, C. Endyana, and Muhammad Aufaristama. "Numerical simulation of non-Newtonian fluid flows through fracture network." In *IOP conference series: earth and environmental science*, vol. 29, no. 1, p. 012030. IOP Publishing, 2016. https://doi.org/10.1088/1755-1315/29/1/012030

[15] Wang, Min, Yi-Feng Chen, Guo-Wei Ma, Jia-Qing Zhou, and Chuang-Bing Zhou. "Influence of surface roughness on nonlinear flow behaviours in 3D self-affine rough fractures: Lattice Boltzmann simulations." *Advances in water resources* 96 (2016): 373-388. https://doi.org/10.1016/j.advwatres.2016.08.006

[16] Zhang, Min, Maša Prodanović, Maryam Mirabolghasemi, and Jianlin Zhao. "3D microscale flow simulation of shear-thinning fluids in a rough fracture." *Transport in Porous Media* 128 (2019): 243-269. https://doi.org/10.1007/s11242-019-01243-9

[17] Tian, Xu, Yinger Deng, Dang Jing, Xin Peng, and Mubai Duan. "Research on the influence of geometry on nonlinear flow in constructed rough fractures by lattice Boltzmann simulation." *Arabian Journal of Geosciences* 13 (2020): 1-18. https://doi.org/10.1007/s12517-019-5051-3

[18] Irayani, Z., U. Fauzi, S. Viridi, and F. D. E. Latief. "Calculation of anisotropy permeability from 3D tomographic images using renormalization group approaches and lattice Boltzmann method." *Journal of Petroleum Exploration and Production Technology* 9 (2019): 889-897. https://doi.org/10.1007/s13202-018-0558-9

[19] Niya, SM Rezaei, and A. P. S. Selvadurai. "Correlation of joint roughness coefficient and permeability of a fracture." *International Journal of Rock Mechanics and Mining Sciences* 113 (2019): 150-162. https://doi.org/10.1016/j.ijrmms.2018.12.008

[20] Yin, Peijie, Can Zhao, Jianjun Ma, and Linchong Huang. "A unified equation to predict the permeability of rough fractures via lattice Boltzmann simulation." *Water* 11, no. 5 (2019): 1081. https://doi.org/10.3390/w11051081

[21] Chaabane, Raoudha, Nor Azwadi Che Sidik, and Abdelmajid Jemni. "Convective Boundary Conditions Effect on Cylindrical Media with Transient Heat Transfer." *Journal of Advanced Research in Fluid Mechanics and Thermal Sciences* 82, no. 2 (2021): 146-156. https://doi.org/10.37934/arfmts.82.2.146156

[22] Zhao, Huawei, Zhengfu Ning, Qinjun Kang, Li Chen, and Tianyi Zhao. "Relative permeability of two immiscible fluids flowing through porous media determined by lattice Boltzmann method." *International Communications in Heat and Mass Transfer* 85 (2017): 53-61. https://doi.org/10.1016/j.icheatmasstransfer.2017.04.020

[23] Sidik, Nor Azwadi Che, Raoudha Chaabane, and Hong Wei Xian. "Heat Transfer Study in Cylindrical Cavity with Heat Absorption or Generation." *Journal of Advanced Research in Applied Sciences and Engineering Technology* 27, no. 2 (2022): 16-27. https://doi.org/10.37934/araset.27.2.1627

[24] Xiao, Feng, and Xiaolong Yin. "Geometry models of porous media based on Voronoi tessellations and their porosity–permeability relations." *Computers & Mathematics with Applications* 72, no. 2 (2016): 328-348. https://doi.org/10.1016/j.camwa.2015.09.009

[25] Zhao, Yanlong, Zhiming Wang, Quanshu Zeng, Jiangtao Li, and Xiao Guo. "Lattice Boltzmann simulation for steady displacement interface in cementing horizontal wells with eccentric annuli." *Journal of Petroleum Science and Engineering* 145 (2016): 213-221. https://doi.org/10.1016/j.petrol.2016.04.005

[26] Jin, Yi, Jiabin Dong, Xiangyu Zhang, Xiang Li, and Ying Wu. "Scale and size effects on fluid flow through self-affine rough fractures." *International Journal of Heat and Mass Transfer* 105 (2017): 443-451. https://doi.org/10.1016/j.ijheatmasstransfer.2016.10.010

[27] Ávila, Joseph, Javier Pagalo, and Mayken Espinoza-Andaluz. "Evaluation of geometric tortuosity for 3D digitally generated porous media considering the pore size distribution and the A-star algorithm." *Scientific Reports* 12, no. 1 (2022): 19463. https://doi.org/10.1038/s41598-022-23643-6

[28] Muntashir, A. W. and Irwan Ary D."Smartfract" *SmartFract*, 2015, http:/grid.unpad.ac.id/~smartfract2/.

[29] Madadi, Mahyar, Clinton D. VanSiclen, and Muhammad Sahimi. "Fluid flow and conduction in two-dimensional fractures with rough, self-affine surfaces: A comparative study." *Journal of Geophysical Research: Solid Earth* 108, no. B8 (2003). https://doi.org/10.1029/2002JB002332

[30] Odling, Noelle E. "Natural fracture profiles, fractal dimension and joint roughness coefficients." *Rock mechanics and rock engineering* 27 (1994): 135-153. https://doi.org/10.1007/BF01020307

[31] Schmittbuhl, J., A. Steyer, L. Jouniaux, and Renaud Toussaint. "Fracture morphology and viscous transport." *International Journal of Rock Mechanics and Mining Sciences* 45, no. 3 (2008): 422-430. https://doi.org/10.1016/j.ijrmms.2007.07.007

[32] Auradou, Harold. "Influence of wall roughness on the geometrical, mechanical and transport properties of single fractures." *Journal of Physics D: Applied Physics* 42, no. 21 (2009): 214015. https://doi.org/10.1088/0022-3727/42/21/214015

[33] Karpyn, Zuleima, Christopher Landry, and Masa Prodanovic. 'Induced Rough Fracture in Berea Sandstone Core'. Digital Rocks Portal, 2016. https://doi.org/10.17612/P7J012

[34] Latt, Jonas, Orestis Malaspinas, Dimitrios Kontaxakis, Andrea Parmigiani, Daniel Lagrava, Federico Brogi, Mohamed Ben Belgacem *et al.*, "Palabos: parallel lattice Boltzmann solver." *Computers & Mathematics with Applications* 81 (2021): 334-350. https://doi.org/10.1016/j.camwa.2020.03.022

[35] Azmi, Mohd Irwan Mohd, Nor Azwadi Che Sidik, Yutaka Asako, Wan Mohd Arif Aziz Japar, Nura Muaz Muhammad, and Nadlene Razali. "Numerical Studies on PCM Phase Change Performance in Bricks for Energy-Efficient Building Application–A Review." *Journal of Advanced Research in Numerical Heat Transfer* 1, no. 1 (2020): 13-21.

[36] Huang, Haibo, Michael Sukop, and Xiyun Lu. "Multiphase lattice Boltzmann methods: Theory and application." (2015). https://doi.org/10.1002/9781118971451

[37] Sukop, M. C. "DT Thorne, Jr. Lattice Boltzmann Modeling Lattice Boltzmann Modeling." (2006). https://doi.org/10.1007/978-3-540-27982-2

[38] Guiltinan, Eric J., Javier E. Santos, M. Bayani Cardenas, D. Nicolas Espinoza, and Qinjun Kang. "Two-Phase Fluid Flow Properties of Rough Fractures With Heterogeneous Wettability: Analysis With Lattice Boltzmann Simulations." *Water Resources Research* 57, no. 1 (2021): e2020WR027943. https://doi.org/10.1029/2020WR027943